

Preparation of Shape-Stabilized Phase Change Material by the Valorization of Oil Palm Waste: Reduced Graphene Oxide-activated Carbon Derived Carbon Matrix for Thermal Energy Storage

Salisu Nasir,^{a,b,c,*} Mohd Zobir Hussein,^{a,*} Zulkarnain Zainal,^c and Nor Azah Yusof^c

A shape-stabilized composite phase change material (SCPCM) made of n-nonadecane infused by capillary forces in a compressed reduced graphene oxide-activated carbon matrix (EFB(rGOAC)-M) was prepared from oil palm empty fruit bunch. The composite exhibited improved thermal properties and was used to fabricate an SCPCM by impregnation, in which the pores of the EFB(rGOAC)-M served as the support, while n-nonadecane was the central envelope. The EFB(rGOAC)-M exhibited a specific surface area of 680 m² g⁻¹ and an average pore size of 22 Å. The successful infiltration of n-nonadecane into the pores of EFB(rGOAC)-M was confirmed *via* nitrogen gas adsorption-desorption isotherms and scanning electron micrographs. According to the differential scanning calorimeter analysis, the composite SCPCM-5 exhibited melting and freezing temperatures of 37.25 °C and 25.58 °C, respectively, and an associated latent heat value of 82.72 J g⁻¹ and -62.22 J g⁻¹, respectively. There was no seepage during the phase change process (from solid to liquid, as the n-nonadecane was uniformly dispersed in the pores of the carbon matrix (EFB(rGOAC)-M) and held by the capillary and the surface tension forces of the carbon matrix. This innovative, inexpensive and environmentally friendly shape-stabilized phase change material could be applied for thermal energy storage applications.

Keywords: Porous carbon matrix; n-Nonadecane; Encapsulation; Shape-stabilized composite; Phase change material; Latent heat; Thermal energy storage

Contact information: a: Materials Synthesis and Characterization Laboratory (MSCL), Institute of Advanced Technology (ITMA), Universiti Putra Malaysia, 43400 Serdang, Selangor, Malaysia; b: Department of Chemistry, Faculty of Science, Federal University Dutse, 7156 Dutse, Jigawa State, Nigeria; c: Department of Chemistry, Faculty of Science, Universiti Putra Malaysia, 43400 Serdang, Selangor, Malaysia; *Corresponding authors: salisunasirbbr@gmail.com; mzobir@upm.edu.my

INTRODUCTION

The most significant challenges facing humanity involve energy, environmental, economic, or security (terrorism) related problems. It is projected that global energy consumption will rise by 48% between 2012 and 2040 (U.S. Energy Information Administration 2016). Currently, about 30% of the total global energy demand comes from the building industry (Cui *et al.* 2014; Dong *et al.* 2016; Yang *et al.* 2017). This sector has garnered global attention from researchers, technologists, and policymakers to reduce the demand or provide an alternative for energy storage and conversion, especially building energy conservation. Novel and sustainable strategies are required to resolve the challenges of future energy demand (due to rapidly growing global population) and environmental

effects (caused by fossil fuel exploitation) (Abbasi and Abbasi 2011; Zhao *et al.* 2019). These advancements in green/renewable technologies should decrease greenhouse gases and the release of noxious materials (Nasir *et al.* 2019). This is in line with the proclamation made in the 72nd United Nations (UN) general assembly of 2017 that the planet Earth is endangered, but it could be relatively safe if the mean global temperature rise could stay below 2 °C, which could be achieved if all countries reduce their greenhouse gas (CO₂, CH₄, *etc.*) emissions generated from fossil-fuel combustion. To systematically end the use of fossil fuels, there are numerous alternatives that harness and store renewable energy supplied by the sun, geothermal, water, wind or biomass sources. However, the major challenge is that the resources considered appropriate to accomplish this mission have to be cost-effective, industrially viable, renewable, and consistently scalable to surpass the performance of existing technologies (White 2015).

Interestingly, the storage of thermal energy occurs in a variety of forms, such as the latent heat of fusion, sensible heat stored in a liquid or solid medium, and chemical energy formed as a result of the reversible chemical reaction. Currently, latent heat thermal energy storage is preferred because it is completely based on phase change materials (PCMs). PCMs have the special ability to store and release energy *via* thawing and solidification. These processes are generally influenced or controlled by the surrounding temperature. PCM-related technology was introduced to improve internal building comfort (temperature) and reduce energy consumption. This technology has attracted attention from various fields due to the high energy storage density and capacity of the PCMs to store energy at a nearly constant temperature.

Since the advent of this technology, various organic and inorganic materials have been exploited for phase change-related applications, such as fatty acids/esters, polyalcohol, paraffin wax (n-alkanes), metals, salts, salt hydrates, and alloys (Zhang *et al.* 2009; Khadiran *et al.* 2015, 2016). However, preference is given to n-alkanes with a general formula of C_nH_{2n+2}, especially n-hexadecane, n-octadecane, and n-nonadecane, because these substances exhibit self-nucleating properties, slight or no supercooling, and high heat of fusion. Their melting and freezing points fall within the human tolerable temperature zone, and they are chemically and thermally stable (Zhang *et al.* 2009; Nasir *et al.* 2019).

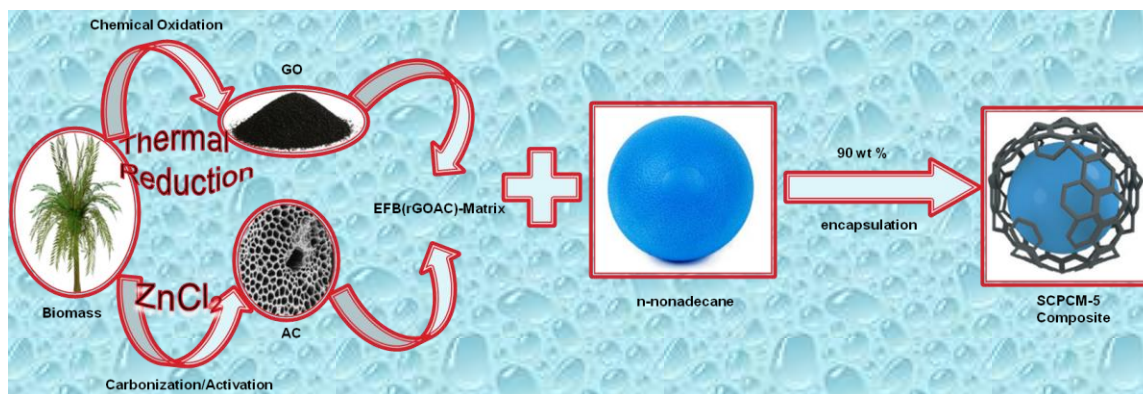


Fig. 1. Schematic representation of the preparation of shape-stabilized phase change material (SCPCM-5) by infiltration of n-nonadecane into the pores of reduced graphene oxide-activated carbon matrix, derived from the oil palm waste precursor.

These properties, especially the higher energy storage density and capacity of the PCMs to store energy at an almost constant temperature, could be sufficient for this emerging technology. Despite all these qualities, paraffin wax has shown evidence of low thermal conductivity, poor heat exchange, and large volume changes (which could cause leakage), which limits the rates of energy storage and release during the thawing and solidification processes. Consequently, for paraffin wax (n-alkanes) to be utilized in PCMs, a thermal conductivity enhancer (TCE) or shape-stabilized phase change materials (SPCMs) should be incorporated (as portrayed in Fig. 1).

Activated carbon (AC) is an appropriate material to provide PCM with both superior thermal conductivity and form-stability (Chen *et al.* 2012; Waisi *et al.* 2019). The porous structure of AC is the central player in tailoring the behaviour and feature of shape-stabilized PCM (Hussein *et al.* 2015). To minimize enthalpy loss for shape stabilized PCM application, AC pores with micro- and nano-meter sizes are widely utilized. Nevertheless, it is not always straightforward to obtain the pore structure of AC with similar pore size distribution, geometrical shape, and network-inner-connected; this is attributed to several factors such as carbon source or precursor used and the general method of activation (González-García *et al.* 2013). For this reason, the study of the thermal energy storage capacity of PCM in the pores of AC is challenging. In this research, AC, reduced graphene oxide (rGO), and their composite were produced using the lignocellulosic-derived materials from oil palm empty fruit bunch. As an abundant waste in Southeast Asia, it is an inexpensive and sustainable carbon precursor for carbon-based materials fabrication. The main goals of this study were to optimize the procedure, modify the low-cost rGO-AC carbon matrix with enhanced or suitable pore structures, and use it as an inorganic framework for the production of shape-stable PCM for thermal energy storage (TES).

Any substance that can absorb, accumulate, and discharge heat in the form of thermal energy is classified as PCM. Thermal energy is stockpiled in the PCM and eventually recovered during the freezing process (Khadiran *et al.* 2016). This concept is understood by studying the impact of rising and falling of the surrounding temperature where the PCM is situated. For instance, when the heat coming from the surroundings exceeds a thawing temperature of PCM, the bonds holding the PCM will ultimately rupture, and the PCM will take up the heat in the endothermic process. When the surrounding temperature falls below the thawing temperature of PCM, the PCM will consequently discharge out the heat in the exothermic process, and as a result, convert to a freezing or solid state (Khadiran *et al.* 2016). These interesting properties of PCMs have led to their application as advanced energy storage materials in building with low thermal mass to preserve and enhance its in-house comfort. Many other important applications are reported for heat regulation of electronics, solar energy, and waste heat recovery (Feng *et al.* 2011).

The smart shape-stabilized phase change composite materials (SCPCM) developed in this study are feasible options to reduce the energy consumption of buildings. This is possible because when material changes phase within a particular temperature range, heat is stored and released. This phenomenon generally increases the building inertia, decreases the temperature flux, and makes the indoor climate very steady. As a result, the inner building temperature will fall within the human comfort zone (thermally comfortable) that does not necessarily require any cooling or heating system, which in turn reduces energy consumption. When electricity consumption is minimized, the demand for fossil fuels decreases, leading to reduced greenhouse gas emissions, which is one of the global efforts towards sustainable development.

The higher energy density exhibited by the PCM is generally ascribed to the latent heat of fusion. Even when there is no considerable change in the measured temperature, it is pragmatic that huge amount of energy is absorbed and discharged when materials change phase (Whiffen and Riffat 2013). The variation in the intermolecular forces between the phases is the main driver that influences the change in energy.

Despite multitude studies on PCMs, rGO, and AC, there has been limited research on the use of the rGO-AC matrix (derived from lignocellulosic feedstock) in PCMs. Most reports used paraffin waxes encapsulated in the porous cavity of the activated carbon derived from other sources (*e.g.*, peat soil). It is informative to observe that the mean pore size of the material plays an influential role in SCPCM performance. For example, a slow molecular motion of the PCMs is usually caused if the pore size is very small, which affects the latent heat storage capacity. Similarly, it is also imperative to retain the PCM during the latent heat storage process by an adequate capillary force action. If the average pore size is too large, the capillary force will not be enough to retain the liquid PCM during the phase change. Consequently, leakage and lower thermal conductivity of pure PCMs have discouraged their widespread applications. Several techniques have been introduced to address these drawbacks. One of the principal methods is incorporating a form-stable material with PCMs to form a composite.

In the present study, a mixture of the lignocellulosic-based rGO and activated carbon with tunable pore size distributions and suitable thermal capacity was designed and prepared for stabilizing the shape of the PCM. This material has been proven useful for the outstanding performance of the phase change system.

EXPERIMENTAL

Materials

Zinc chloride (ZnCl_2) (SystemChemAR, Shah Alam, Malaysia), ethyl alcohol (99.7%) (RandM Chemicals, Semenyih, Malaysia), n-nonadecane (99%) (Sigma-Aldrich, St. Louis, MO, USA), and deionized water were utilized. The empty fruit bunch (EFB) was obtained from the Seri Ulu Langat Palm Oil Mill, Dengkil, Selangor, and was utilized as the starting raw material for the reduced graphene oxide and activated carbon. It was washed thoroughly with deionized water to remove dust particles, oven-dried at 100 °C, and pulverized by a grinder before it was impregnated with activating agents.

Methods

Preparation of reduced graphene oxide using lignocellulosic materials derived from oil palm by-product

As a facile and scalable production process, first, graphene oxide was prepared as described by Marcano *et al.* (2010), with a slight modification as previously reported (Nasir *et al.* 2017, 2018). Briefly, the EFB-derived graphite-like powder (3 g) was mixed with concentrated $\text{H}_2\text{SO}_4/\text{H}_3\text{PO}_4$ (360:40 mL), and 18 g of KMnO_4 was gradually added to the mixture, raising the temperature of the reaction mixture to 35 to 40 °C. The mixture was kept under controlled stirring for 12 h at 50 °C. The reaction was allowed to cool to room temperature, and 400 mL of icy-deionized-water was poured concurrently with 3 mL of 30% H_2O_2 . It was then washed and filtered with 200 mL of water, 200 mL of 30% HCl, and 200 mL of ethanol. This process was repeated twice, and the GO was obtained by grouping the particles together with 200 mL of ether and finally dried overnight at room

temperature. The as-fabricated GO was later deoxygenated to graphene-like material (in the form of the reduced graphene oxide) through thermal treatment using a low-temperature annealing reduction method. This process was done at 300 °C in a furnace under the controlled steady flow rate of high purity N₂ at 150 cm³/min.

Preparation of the empty fruit bunch-derived activated carbon

The ZnCl₂ activation step of the waste EFB was performed as follows: typically, 10 g of the pulverized EFB was impregnated with different concentrations (0, 11, 22, and 33% w/w) of ZnCl₂ by stirring in an aqueous solution of the said chemical. This was followed by an evaporation step at 80 °C. The impregnation ratio was 1:0, 1:1.1, 1:2.2, and 1:3.3, respectively, which by definition is the mass ratio of activating agent to dried samples. The dried EFB/ZnCl₂ mixture was then carbonized at 900 °C for 3 h at a heating rate of 10 °C/min under nitrogen atmosphere. Carbonization was performed to purge low-melting-point and low-boiling-point organic compounds leading to carbon with a surface area and good pore size distribution. Following the carbonization, the resulting activated carbon samples were further pulverized, using mortar and pestle. The sample was repeatedly washed (refluxes) with 1 L of 3 M HCl solution and later with deionized water in order to remove the remnant of the ZnCl₂ and attain a neutral pH value. The sample was activated at 500 °C, and the final product was designated as activated empty fruit bunch (EFBAC-0, EFBAC-11, EFBAC-22, and EFBAC-33), where 0, 11, 22, and 33 were corresponding to the ZnCl₂ treatment concentrations, respectively.

Preparation of reduced graphene oxide-activated carbon matrix EFB(rGOAC)-M

Graphene oxide and reduced graphene oxide have applications in composite materials due to their 2D structure and excellent properties (Hazra and Basu 2016). In this study, a template or matrix of these materials was formed as follows. An equal ratio (3 g each) of the rGOEFB and EFBAC-22 were mixed, homogenized, and ground together. The composite mixture was refluxed in 1 L deionized water overnight and subsequently ultrasonicated for 6 h. After drying in an oven, the composite was reactivated in the furnace at 300 °C under a controlled flow rate of high purity nitrogen gas before encapsulation with n-nonadecane. The graphitic composite materials retained several of the properties of the rGOEFB and the physicochemical properties of the activated carbon (EFBAC-22) sample.

Preparation of shape-stabilized n-nonadecane/ EFB(rGOAC)-M composites (SCPCMs)

The shape-stabilized phase change material (SCPCM) was synthesized by a simple impregnation process. n-Nonadecane with the melting point of 32 °C was selected as the phase change material, while reduced graphene oxide-activated carbon matrix [EFB(rGOAC)-M] derived from the EFB feedstock was used as supporting material. Initially, the n-nonaadecane (C₁₉H₄₀) was heated to slightly above its melting temperature (32 °C). The resulting melted C₁₉H₄₀ was dissolved in 30 mL of absolute ethanol. The reduced graphene oxide-activated carbon matrix EFB(rGOAC)-M was added into the n-nonadecane solution, and the mixture was stirred at 500 rpm for 4 h. Finally, the mixture was oven-dried at 80 °C for two days to evaporate all residual ethanol. The content of the n-nonadecane in the composite PCM was varied from 10, 30, 50, 70, and 90 wt%, (Table 1). The prepared materials were stored in sample bottles.

Table 1. n-Nonadecane and EFB(rGOAC)-M Compositions Utilized for the Production of the Shape-stabilized n-Nonadecane/EFB(rGOAC)-M Composites

n-Nonadecane/ EFB(rGOAC)-M (wt%)	n-Nonadecane (g)	EFB(rGOAC)-M (g)	Composite Name
10	0.2	2	SCPCM-1
30	0.6	2	SCPCM-2
50	1.0	2	SCPCM-3
70	1.4	2	SCPCM-4
90	1.8	2	SCPCM-5

The efficacy of the encapsulation of the n-nonadecane into the pores of EFB(rGOAC)-M was evaluated by Eq. 1, taking into account the enthalpy of the pure n-nonadecane,

$$\text{PCM amount (wt\%)} = \left(\frac{\Delta H_m}{\Delta H_{\text{pcm}}} \right) \times 100 \quad (1)$$

where ΔH_m is the enthalpy of thawing of the SCPCM composite (J g^{-1}), and ΔH_{pcm} is the enthalpy of thawing for the pure n-nonadecane (J g^{-1}).

One of the drawbacks associated with the organic PCMs, more especially paraffin, for thermal energy storage application is related to their leakage when the PCM melts. For this reason, seepage was evaluated in the prepared composite materials. The SCPCM (precisely SCPCM-5) was kept in the oven at 90 °C for 72 h. To determine the capability of the EFB(rGOAC)-M carbon matrix to clasp the n-nonadecane during the thawing phase, one gram (1 g) of the SCPCM-5 was measured on a filter paper and subjected to 45 °C for 12 h. Afterward, the sample was put in the oven at 90 °C for 72 h, as described earlier. The mass and the latent heat of the composite material after this testing period were evaluated.

Materials characterization

The BET (Brunauer-Emmet-Teller) surface area, total pore volume, and average pore size of the rGOEFB, EFBAC-22% ZC, EFB(rGOAC)-M, and all of the SCPCMs nanocomposites were measured by the nitrogen gas adsorption-desorption method at 77 K (liquid nitrogen temperature) on a Micromeritics Tristar II plus (Norcross, GA, USA). The analysis was also used as a yardstick to validate the encapsulation or impregnation of the n-nonadecane-based PCM into the pores of the as-prepared EFB(rGOAC)-M. Before the experiment; the samples were outgassed at 290 °C for 12 h under vacuum. The BET equation and Barrett-Joyner-Halenda (BJH) methods were applied to evaluate the specific surface area and the pore size distributions of the materials. Fourier transform infrared (FTIR) spectra of the as-prepared materials were generated using a Nicolet 6700 models (Thermo Scientific, Waltham, MA, USA). The pellets were obtained by mixing 1 mg of the sample and 200 mg of potassium bromide (KBr) and compressing the mixture in a manual hydraulic press, and absorbance was recorded from 400 to 4000 cm^{-1} . The graphitic traits of the materials were examined using Raman spectroscopy, with a WiTec Raman spectrometer (WiTec, Ulm, Germany) using a laser excitation wavelength of 532 nm. The intensity ratio between the D-line ($\sim 1350 \text{ cm}^{-1}$) and the G-line ($\sim 1597 \text{ cm}^{-1}$) of the Raman spectra was used as a yardstick for the graphitization condition of the samples. The surface morphology of the materials was observed using a Nova Nanosem 230 field emission scanning electron microscope (FESEM; Hillsboro, OR, USA). Prior to the analysis, the dried samples were disseminated on a conductive carbon adhesive tape surface that was attached to a FESEM stub and then gold-coated using sputter coater equipment.

The melting and freezing temperatures as well as the enthalpy or the latent heat

(generally referred as the thermal energy storage properties) of the pure n-nonadecane and the nanocomposite were investigated by a differential scanning calorimeter (DSC Q20 V24.10 Build 122, TA Instrument, New Castle, DE, USA) equipped with a refrigerated cooling system. Briefly, 6 mg of the sample was placed in an aluminium pan. The experiment was started from -20 to 100 °C for the heating cycle phase and *vice versa* for the cooling cycle stage in a persistent flow of pure nitrogen gas with the flow rate of 50 mL/min. The thermal stability of the SCPCMs was determined by using a TGA Q500 V20.13 Build 39 (TA Instruments, Newcastle, DE, USA). The sample was analyzed under a nitrogen atmosphere from room temperature to 1000 °C with a heating rate of 10 °C/min and flow rate of 20 mL/min.

RESULTS AND DISCUSSION

The materials prepared in the present study were subjected to thorough characterization, and their thermal energy storage potentials were analyzed. The results are discussed in detail below.

Structure and Chemical Characterization of Empty Fruit Bunch-based Reduced Graphene Oxide-Activated Carbon Matrix

The chemical analysis of the raw EFB and its resulting rGO (acquired after chemical oxidation and thermal reduction processes), and activated carbon (acquired after ZnCl₂ treatment and carbonization-activation process) was done using FTIR spectroscopy, and the results are presented in Figs. 2 and 3. The detailed information on the interactions between the components of the composite was revealed using the same analysis (Fig. 4).

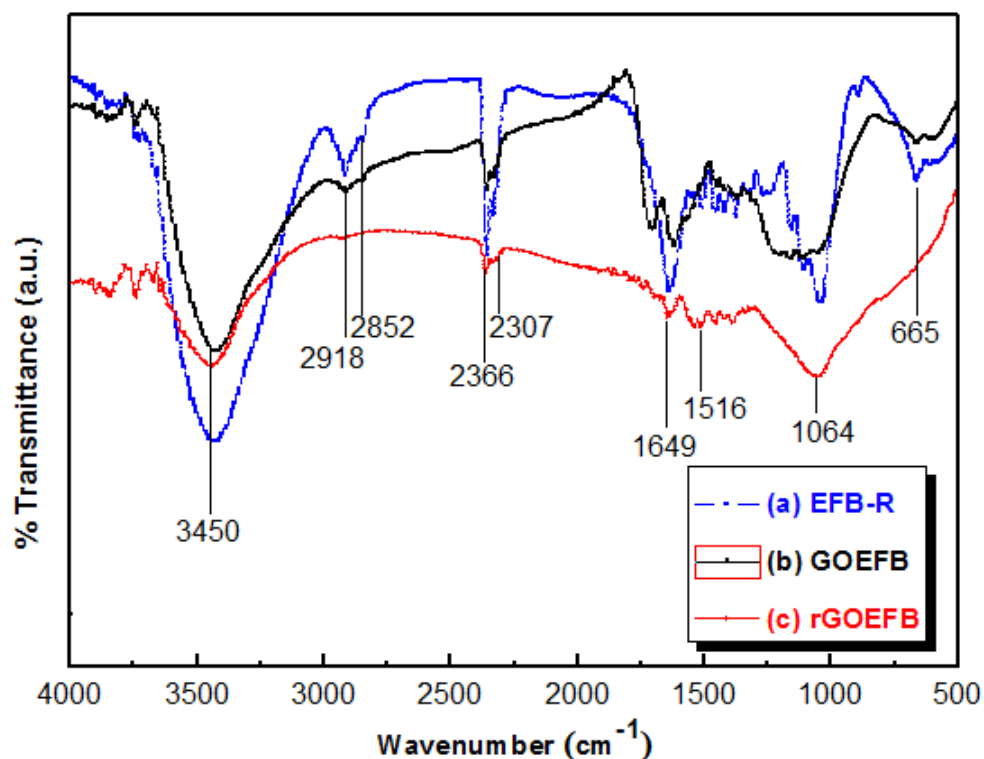


Fig. 2. FTIR spectra of (a) raw empty fruit bunch sample, (b) graphene oxide derived from empty fruit bunch precursor (c) reduced graphene oxide derived from empty fruit bunch precursor

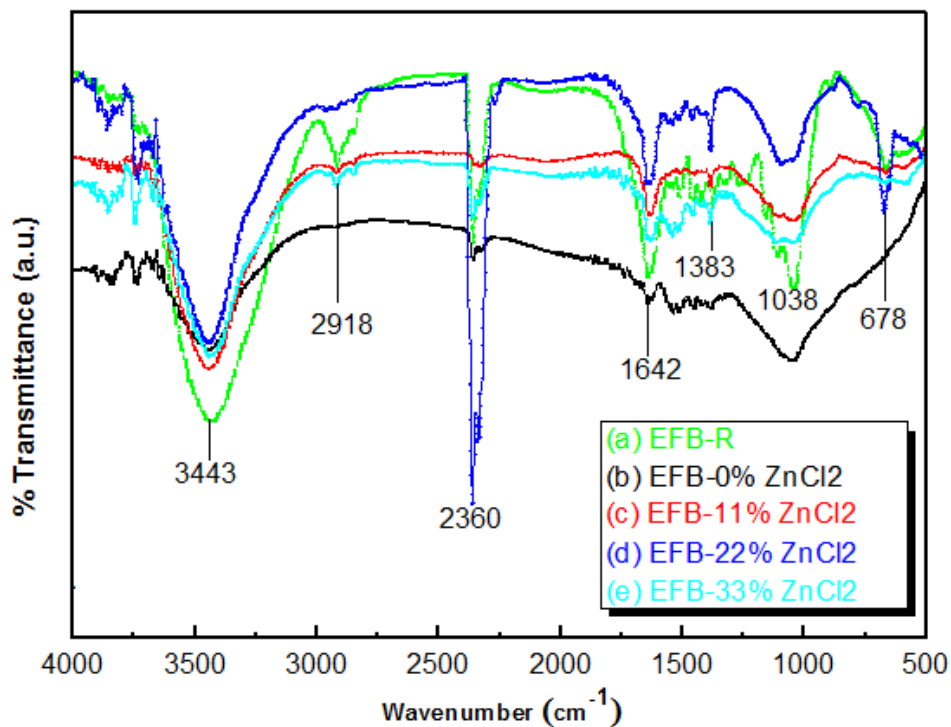


Fig. 3. FTIR spectra of the raw empty fruit bunch sample and its corresponding activated carbon prepared using different concentrations of zinc chloride

Based on the spectra in Figs. 2 and 3, the raw EFB sample exhibited several absorption peaks in the fingerprint region between 1649 and 665 cm^{-1} (Fig. 2) and 1642 and 678 cm^{-1} (Fig. 3) as compared to its corresponding GO, rGO, and activated carbon, respectively. The occurrence of those multiple absorption peaks is an indication of extra chemical functional groups (mostly primary aliphatic alcohol, esters, and aliphatic hydrocarbons) in the raw EFB samples. After the modification and conversion of the raw EFB feedstock into GO, rGO, and activated carbon, the surface functional groups had been converted to an aliphatic carboxylic acid, aliphatic hydrocarbons, and secondary aliphatic alcohols.

In Fig. 4, the characteristic absorption peak at 2921 and 2851 cm^{-1} are the C-H stretching bands of n-nonadecane. The peaks at 1468 cm^{-1} are ascribed to the CH_2 bending vibrations, whereas the peak at 723 cm^{-1} connotes to the trembling and out-of-plane bending vibration of CH_2 in n-nonadecane. It is apparent from the FTIR spectra of the composite materials (Fig. S.1) that the impregnation of n-nonadecane was partially achieved in 10 and 30 wt%. However, at 50 wt% and above of n-nonadecane concentrations, the impregnation and the contributions of the n-nonadecane to the FTIR spectra of the composite materials were properly observed. The best impregnation or encapsulation was realized at 90 wt% of the n-nonadecane concentration (Fig. S.1).

Interestingly, no shift in the absorption peaks of n-nonadecane was observed in the FTIR spectra of all composite materials. This result is an indication that no chemical interaction occurred between the n-nonadecane and the EFB(rGOAC)-matrix. Thus, the n-nonadecane had been properly adsorbed and disseminated into the pores of reduced graphene oxide-activated carbon matrix, EFB(rGOAC)-M through capillary and surface tension forces. In effect, the problem of seepage of the molten PCM from the composite material was avoided.

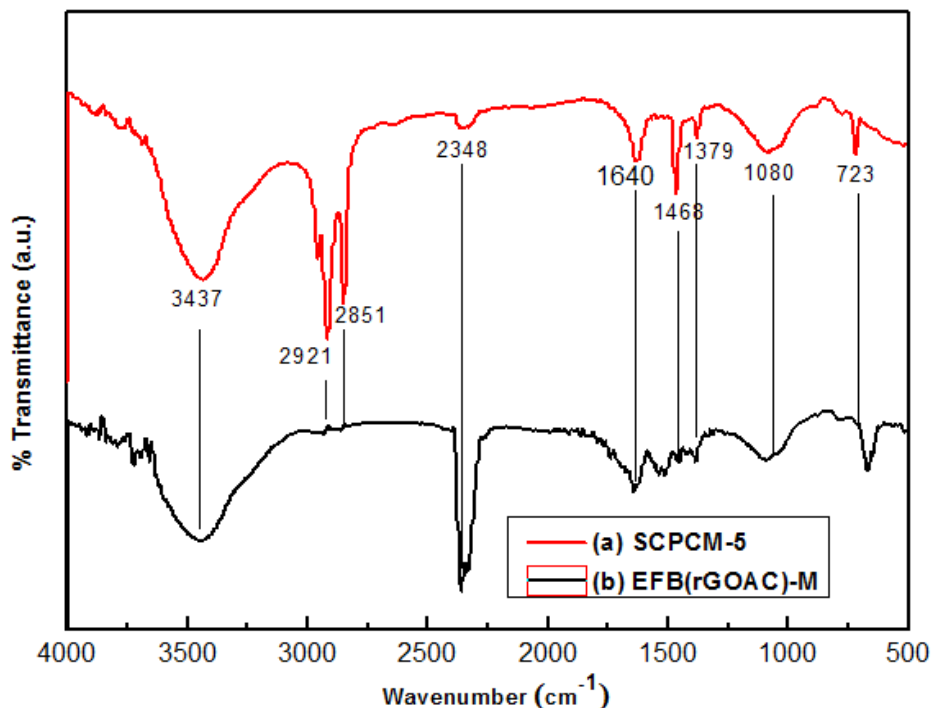


Fig. 4. FTIR spectra of (a) composite SCPCM-5 derived from the combination of reduced graphene oxide, activated carbon, and 90 weight% of n-nonadecane; (b) EFB-derived carbon matrix, made from the mixture of reduced graphene oxide and activated carbon (AC)

Figure 5 shows the Raman spectra of all of the composite SCPCMs, which exhibited two apparent peaks at 1342 and 1581 cm^{-1} . These connote to the D and G bands of disordered and graphitic carbons, respectively. The calculated I_G/I_D ratios of the composite SCPCMs were 1.06, 0.98, 1.06, 1.12, 1.04, for SCPCM-1 (nND-rGOAC 10 wt%), SCPCM-2 (nND-rGOAC 30 wt%), SCPCM-3 (nND-rGOAC 50 wt%), SCPCM-4 (nND-rGOAC 70 wt%), SCPCM-5 (nND-rGOAC 90 wt%), respectively, signifying the amorphous carbon composition coupled with loads of lattice edges or plane defects of EFB(rGOAC)-matrix (Mehrali *et al.* 2016). These structural defects that later metamorphosed into pores during the AC and rGO preparations (due to the influence of the chemical impregnation reagents and activation parameters) drive the adsorption and encapsulation of n-nonadecane during the SCPCM composite formation. The defects developed initially during the contraction and expansion of the ring induced by the thermal decomposition temperature. This inducement sets the atoms into a frequent and random motion, changes their position, and creates an empty lattice site. The vacant spaces produced are the initial place where the atoms are located but changed position during the process, and this leads to the distortion of the structure of the materials. Even though the samples are amorphous, the presence of graphitic cannot be ruled out due to the emergence of the sharp G-peak (Fig. 5) from the Raman spectral analysis. These sharp Raman G-peaks suggest that the samples have sp^2 carbon networks in their structures (Pimenta *et al.* 2007). Thus, it can be summarized from the calculated I_G/I_D values that the sample exhibited the requisite graphitic trait, needed to increase the strength, stiffness, and thermal conductivity ability of the reduced graphene oxide, activated carbon, and the corresponding composite material. For this reason, the EFB(rGOAC)-M becomes very suitable as a support material for n-nonadecane-based PCMs as the thermal energy storage.

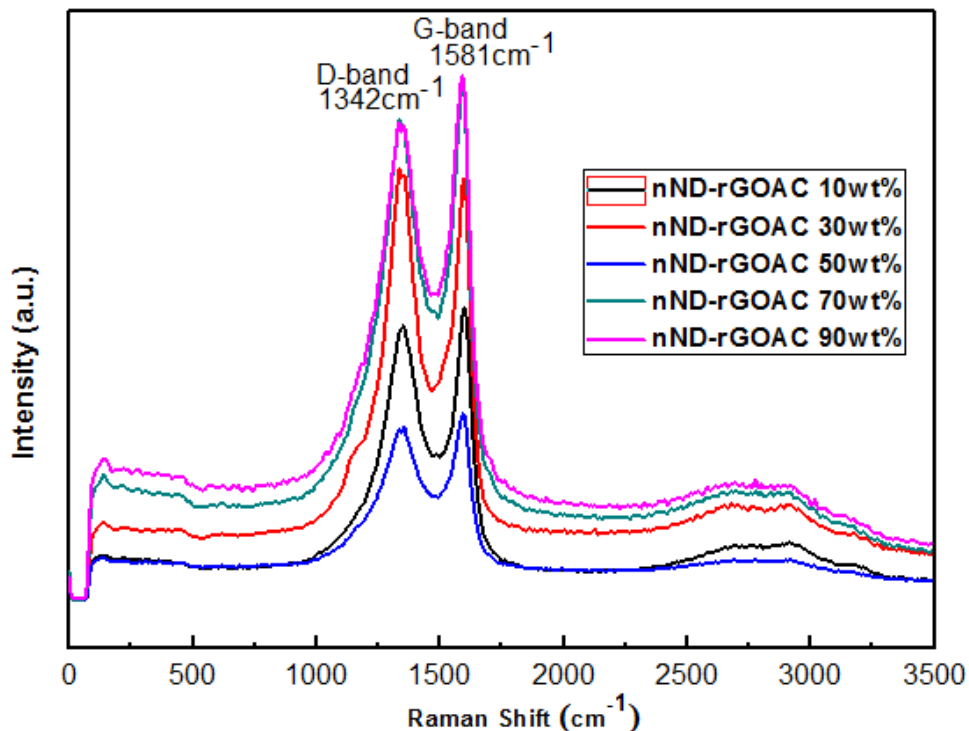


Fig. 5. Raman spectra of composite SCPCMs prepared from the mixture of reduced graphene oxide, activated carbon, and different weight% of n-nonadecane

The microstructure of the representative composite PCM is presented in Fig. 6. Figure 6(a-c) shows the FESEM images of the activated carbon, reduced graphene oxide, and the resulting framework or carbon matrix prepared from them. The morphology of the carbon matrix is marked with a well-established porosity, which supports the result obtained from the nitrogen adsorption/desorption isotherms. The FESEM image in Fig. 6(d) confirms that the n-nonadecane was uniformly dispersed and adsorbed into the network created by EFB(rGOAC)-M used as the framework material. This kind of distribution or dispersion is generally influenced by the capillary effect of the surface tension forces involving n-nonadecane and the porous EFB(rGOAC)-M (Khadiran *et al.* 2015), and it is the main driver that offer mechanical strength to the entire compound (P. Zhang *et al.* 2009). As a result, the material can preserve its original form in the solid state devoid of any leakage of the thawed PCM.

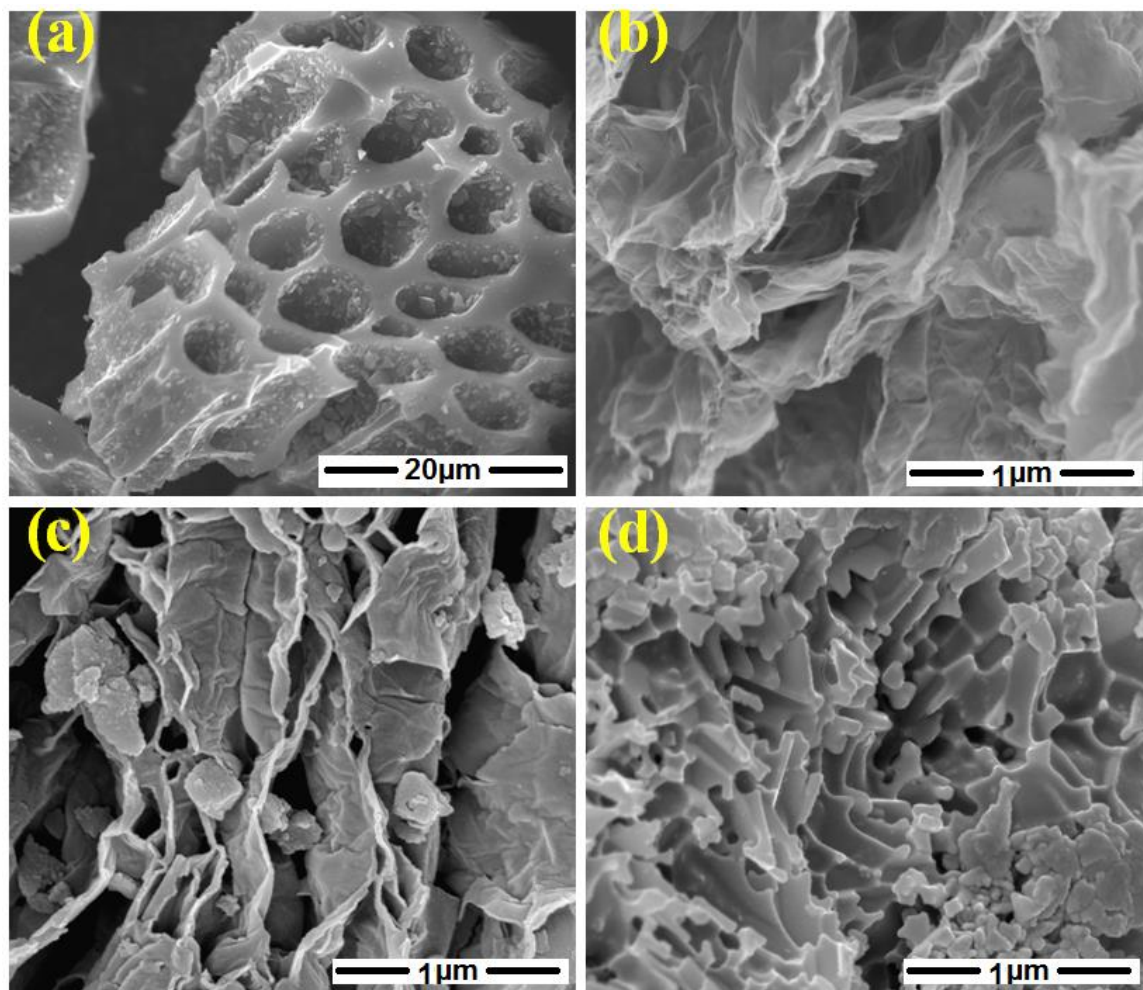


Fig. 6. FESEM images of the (a) EFBAC-22% $ZnCl_2$ -derived activated carbon (b) EFB-derived reduced graphene oxide (rGOEFB) (c) Mixture of (a) and (b) that formed the EFB(rGOAC)-M framework (d) shows the SCPCM-5 which is derived from the impregnation of n-nonadecane into the pores of (c)

Pore Structure and BET Surface Area Analyses

Gas adsorption is a well-established technique for characterizing the texture of porous solids and fine powders (Thommes *et al.* 2015). This technique was applied to confirm the occlusion of the n-nonadecane used as the phase change material into the porous structure of EFB(rGOAC)-M. Interestingly, the occlusion or encapsulation was successfully achieved by taking into account the changes of the pattern (before and after the impregnation process) of both the nitrogen adsorption-desorption isotherms, the pore size distribution of the EFB(rGOAC)-matrix, and the resulting SCPCMs prepared using 50, 70, and 90 wt% (n-nonadecane/ EFB(rGOAC)-M weight ratios), as shown in Figs. 7 and 8. The evolution of the Type I nitrogen adsorption-desorption isotherm of the EFB(rGOAC)-M (Fig. 7a) suggest microporous solids having relatively small external surfaces, with the amount adsorbed moving towards a limiting value. This restrictive uptake is influenced by the susceptible micropore volume instead of internal surface area (Thommes *et al.* 2015).

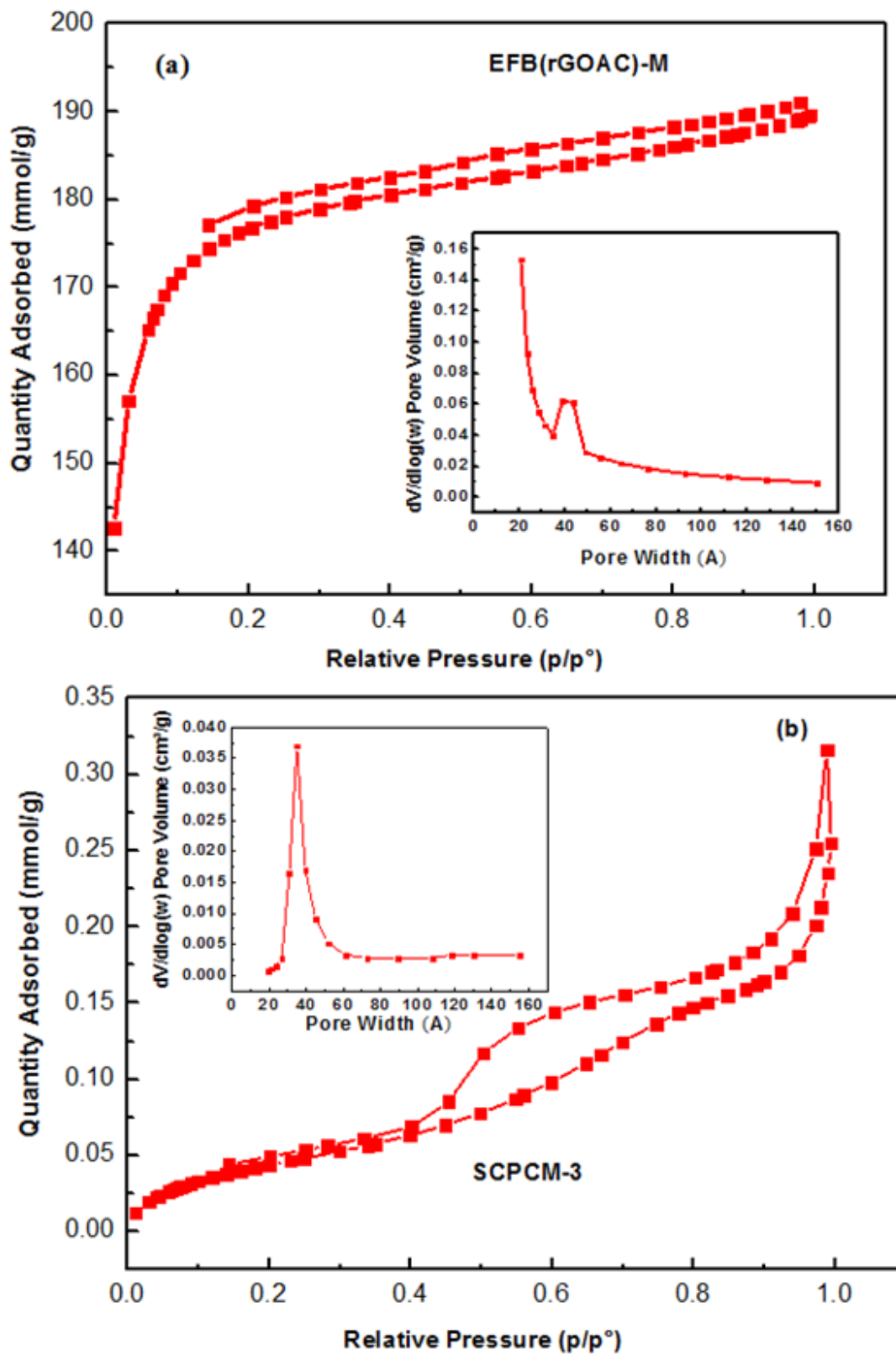


Fig. 7. Nitrogen adsorption-desorption isotherms of (a) EFB(rGOAC)-M, (b) SCPCM-3. Inset indicates their respective pore size distributions.

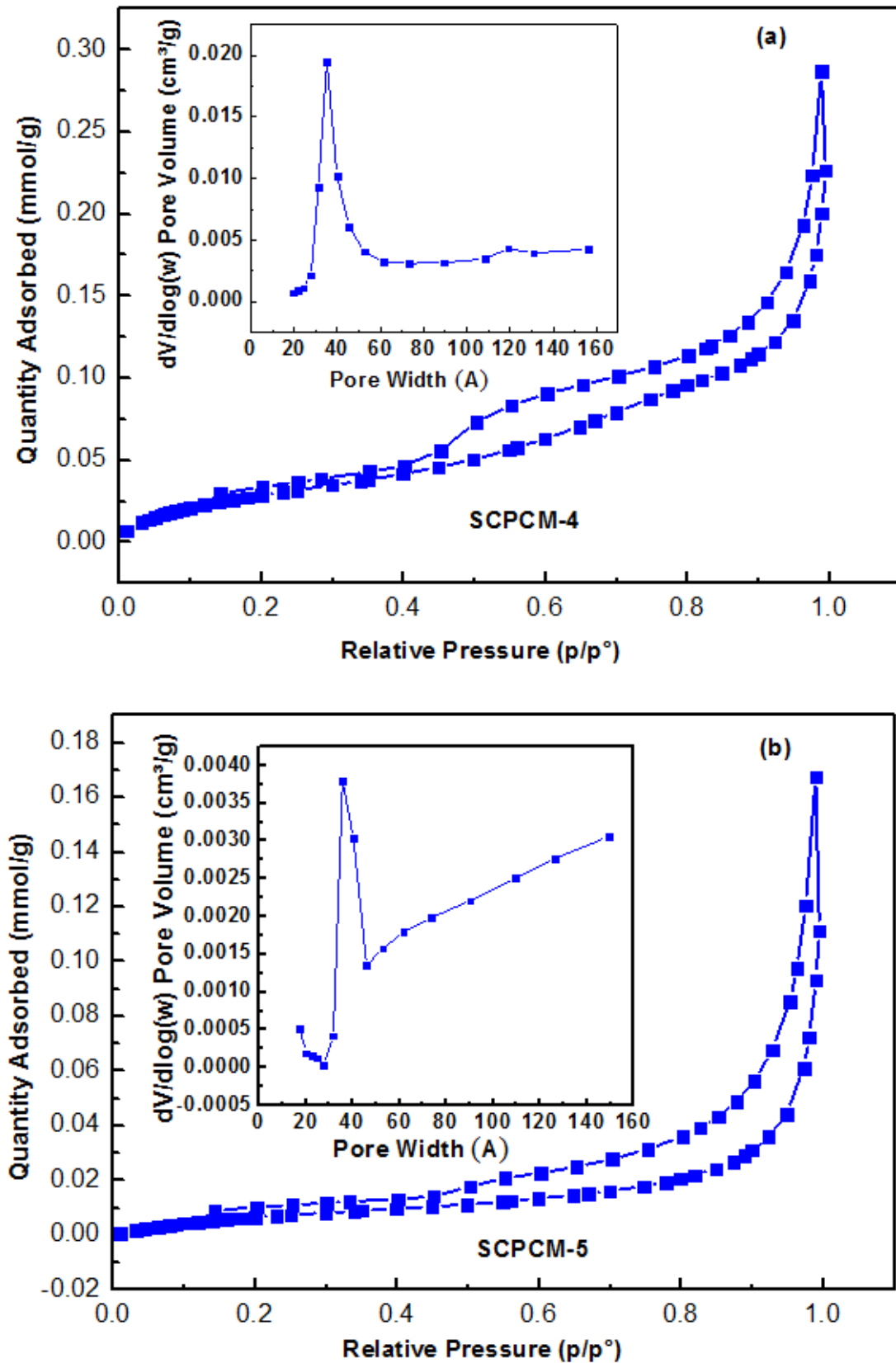


Fig. 8. Nitrogen adsorption-desorption isotherms of (a) SCPCM-4, (b) SCPCM-5. The inset shows their respective pore size distributions.

The nitrogen adsorption-desorption isotherm of both SCPCM-3, SCPCM-4, and SCPCM-5 (Fig. 7b and 8a,b, respectively) are of Type III, having no identifiable monolayer formation, signifying that the SCPCMs had poor chemical reactivity, which led to their low adsorption affinity. Unsurprisingly, the micropores of the carbon matrix in the EFB(rGOAC)-M were completely occluded by the n-nonadecane. Thus, the nitrogen adsorption-desorption affinity of EFB(rGOAC)-M eventually declined by intensifying the n-nonadecane amount and *vice versa* at lower n-nonadecane percentage loading, as in SCPCM-1 and SCPCM-2 (Fig. S.2).

Table 2 shows other informational evidence of the successful penetration of the n-nonadecane into the pores of the EFB(rGOAC)-M carbon matrix. For instance, the BET specific surface area, and total pore volume of the composite PCMs (SCPCM-1, SCPCM-2, SCPCM-3, SCPCM-4, and SCPCM-5) were decreased to 315 m²/g, 22 m²/g, 4 m²/g, 3 m²/g, 1 m²/g; and 0.174 cm³/g, 0.028 cm³/g, 0.005 cm³/g, 0.004 cm³/g, 0.001 cm³/g, respectively, as compared to EFB(rGOAC)-M which was 680 m²/g, and 0.253 cm³/g. In addition, the BJH desorption average pore width of all of the composite SCPCMs (SCPCM-1, SCPCM-2, SCPCM-3, SCPCM-4, and SCPCM-5) were higher than the pore width of EFB(rGOAC)-M carbon matrix which was 32 Å, 36 Å, 42 Å, 47 Å, and 61 Å. This is clear evidence that all of the micropores of the EFB(rGOAC)-M carbon matrix was fully occupied (filled up) by the n-nonadecane. It can, therefore, be concluded that the encapsulation or rather infiltration had occurred, which is consistent with the pattern of previously reported literature (Khadiran *et al.* 2015).

Table 2. Surface Properties of the Porous EFB(rGOAC)-M Compared with the SCPCMs Formed after Impregnation with Different Weight Percentages of n-Nonadecane

	EFB(rGOAC)-M	SCPCM-1	SCPCM-2	SCPCM-3	SCPCM-4	SCPCM-5
BET Surface Area (m ² /g)	680	315	22	4	3	1
n-nonadecane Loading (%)	-	1	6	18	26	36
BJH Desorption Average Pore Width (Å)	30	32	36	42	47	61
DFT Total Volume in Pores (cm ³ /g)	0.2530	0.1736	0.0279	0.0052	0.0035	0.0008
Isotherm Classification	Type I	Type IV	Type III	Type III	Type III	Type III

Based on the percentage loading of the PCM (Table 2) which was calculated by dividing the latent heat of melting of the SCPCM by that of the pure n-nonadecane multiplied by 100, the presence of n-nonadecane on the surface of EFB(rGOAC)-M carbon matrix can be highly promulgated. The amount may be perceived as inconsequential, as exhibited by most of the SCPCMs; however, its influence has consequentially circumvented the n-nonadecane from leaching out even for the composite with higher n-nonadecane composition, as in SCPCM-5. SCPCM-5 and SCPCM-3 were chosen for subsequent experiments.

Thermal Energy Storage Performance of Oil Palm Waste-based SCPCM Composites

The thermal characteristics of the n-nonadecane and n-nonadecane/EFB(rGOAC)-M composite PCM was investigated using DSC analysis. Figure 9 shows that increasing the concentration of the n-nonadecane increased the heat storage ability of the composite PCM. Thus, the composite PCM prepared from the 90wt% n-nonadecane (SCPCM-5) showed the best energy storage ability as compared to its counterpart.

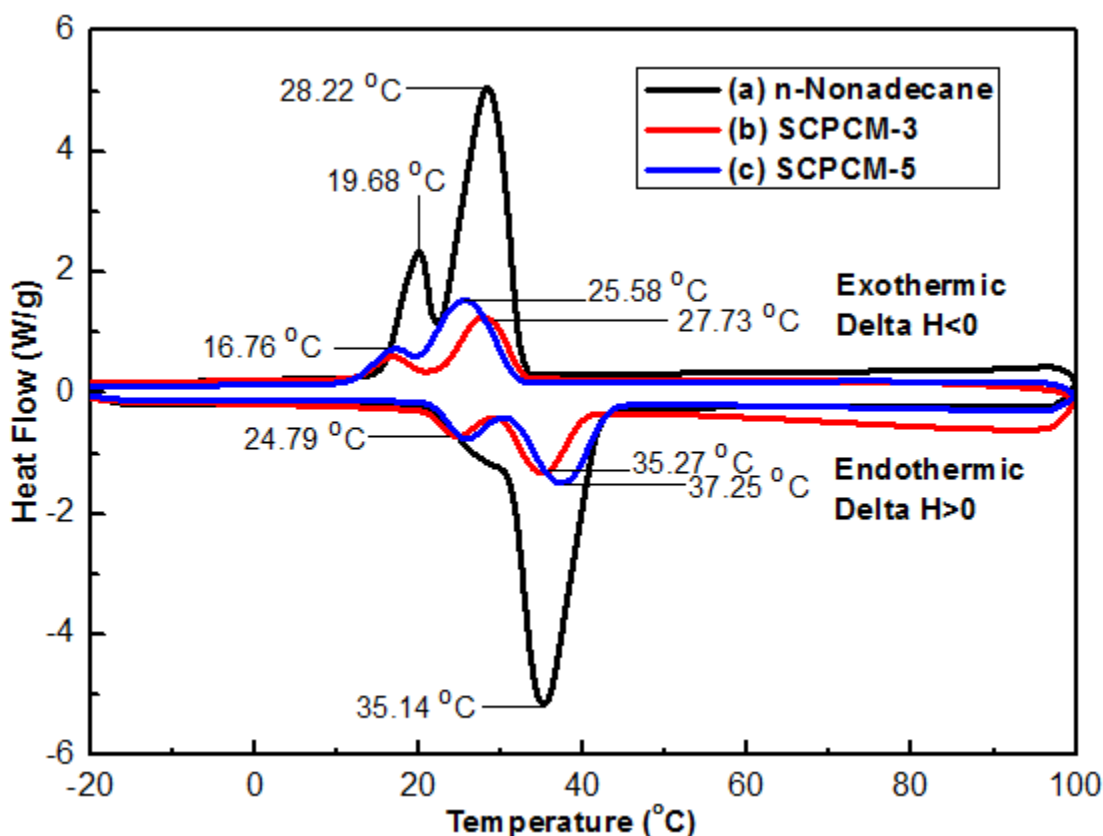


Fig. 9. The differential scanning calorimeter (DSC) thermograms of (a) pure n-nonadecane (b) SCPCM-3 with n-nonadecane mass percentages of 50% (c) SCPCM-5 with n-nonadecane mass percentages of 90%

As shown in Fig. 9a, the DSC curve of n-nonadecane exhibited dual phase change peaks. The major peak that surfaced at 35.14 °C corresponds to the solid–liquid phase change of n-nonadecane, while the parallel one at 28.22 °C represents the solid–solid phase transition of n-nonadecane.

The composite PCMs also exhibited two peaks at 35.27 °C and 27.73 °C (SCPCM-3) and 37.25 °C and 25.58 °C (SCPCM-5). The nearly analogous curves (Fig. 9b, c) signified that the composite SCPCMs (though with different mass fractions of n-nonadecane) had similar thermal properties. Moreover, the solid–liquid phase change temperature of the SCPCM-3 (35.27 °C) was close to that of the n-nonadecane (35.14 °C). The evaluated total latent heats of the n-nonadecane and the SCPCM-3 and SCPCM-5 are given in Table 3.

Table 3. Differential Scanning Calorimeter Data of Pure n-Nonadecane and the SCPCMs Composites

Sample	Mass Fraction (wt%)	Melting		Freezing	
		Thawing peak temperature (°C)	Thawing latent heat ΔH_m (J/g)	Solidification peak temperature (°C)	Solidification latent heat ΔH_f (J/g)
n-Nonadecane	100	35.14	229	28.22	-234
SCPCM-3	50	35.27	40.54	27.73	-38.13
SCPCM-5	90	37.25	82.72	25.58	-62.22

Based on the weight ratio of n-nonadecane in the composite SCPCMs, the latent heats (melting and solidification) were 40.54 J/g and -38.13 J/g (for SCPCM-3) and 82.72 J/g and -62.22 J/g (for SCPCM-5), respectively. These latent heats were lower than pure n-nonadecane. The latent heat of PCM composites can be reduced by carbon-based nanomaterials due to a 3-D net structure that prevents heat movement (Zhang *et al.* 2012; Yu *et al.* 2014). As observed in Table 3, the phase temperatures of n-nonadecane in the composite SCPCMs were considerably affected or controlled by the mass fraction (wt%) of the n-nonadecane. With the increase of the n-nonadecane content, the melting temperature of the composite SCPCM also increased, while the freezing temperature exhibited a reverse tendency. This trait lessens the degree of super-cooling of the composite phase change materials (Zhang *et al.* 2012).

For clarity, the allied latent heats can be classified as endothermic and exothermic processes/reactions. In the course of an endothermic process (*e.g.*, melting), the system receives energy in the form of heat from the surroundings. The temperature of the surroundings decreases (Fig. 9); hence, the enthalpy change is greater than zero ($\Delta H_m > 0$). The exothermic process (solidification/freezing) is precisely opposite to endothermic process, and $\Delta H_m < 0$.

Liquid leakage analysis

There was no indication of seepage after the sample was subjected to 45 °C for 12 h. Both the weight and the latent heat of the SCPCM-5 composite material before and after the leakage assessment remained nearly the same. The weight after it was subjected to 90 °C for 72 h exhibits a decrease of only 5% (about 0.05 g) from the 1 g of the SCPCM-5 utilized in the present investigation. No considerable differences in the latent heats of SCPCM-5 were seen before (82.72 J g⁻¹ and -62.22 J g⁻¹) and after (82.50 J g⁻¹ and -62.05 J g⁻¹) the leakage evaluation. It can be summarized that the potential leakage of the molten n-nonadecane was prevented due to the strength or stability of the carbon matrix. The stability originated from its surface chemistry (due to the chemical functional groups) and the soaring capillary force formed by the covalent bond between the pores of EFB(rGOAC)-M which is holding the n-nonadecane.

Thermal stability of form-stable n-nonadecane/EFB(rGOAC)-M composite PCM (SCPCM-5)

Figure (10a, b) shows the thermal degradation behaviour of EFB(rGOAC)-M and n-nonadecane. The TGA/DTG thermogram of EFB(rGOAC)-M exhibited no thermal disintegration below 500 °C. The thermal decay of this sample occurred at 556 °C, with a weight loss of about 4.15%, representing the decomposition of lignin in the reduced

graphene-activated carbon matrix derived EFB precursor (Fig. 10a). The reduced graphene oxide-activated carbon matrix (EFB(rGOAC)-M) is thermally stable (up to 556 °C). For this reason, it was used as supporting material for PCM.

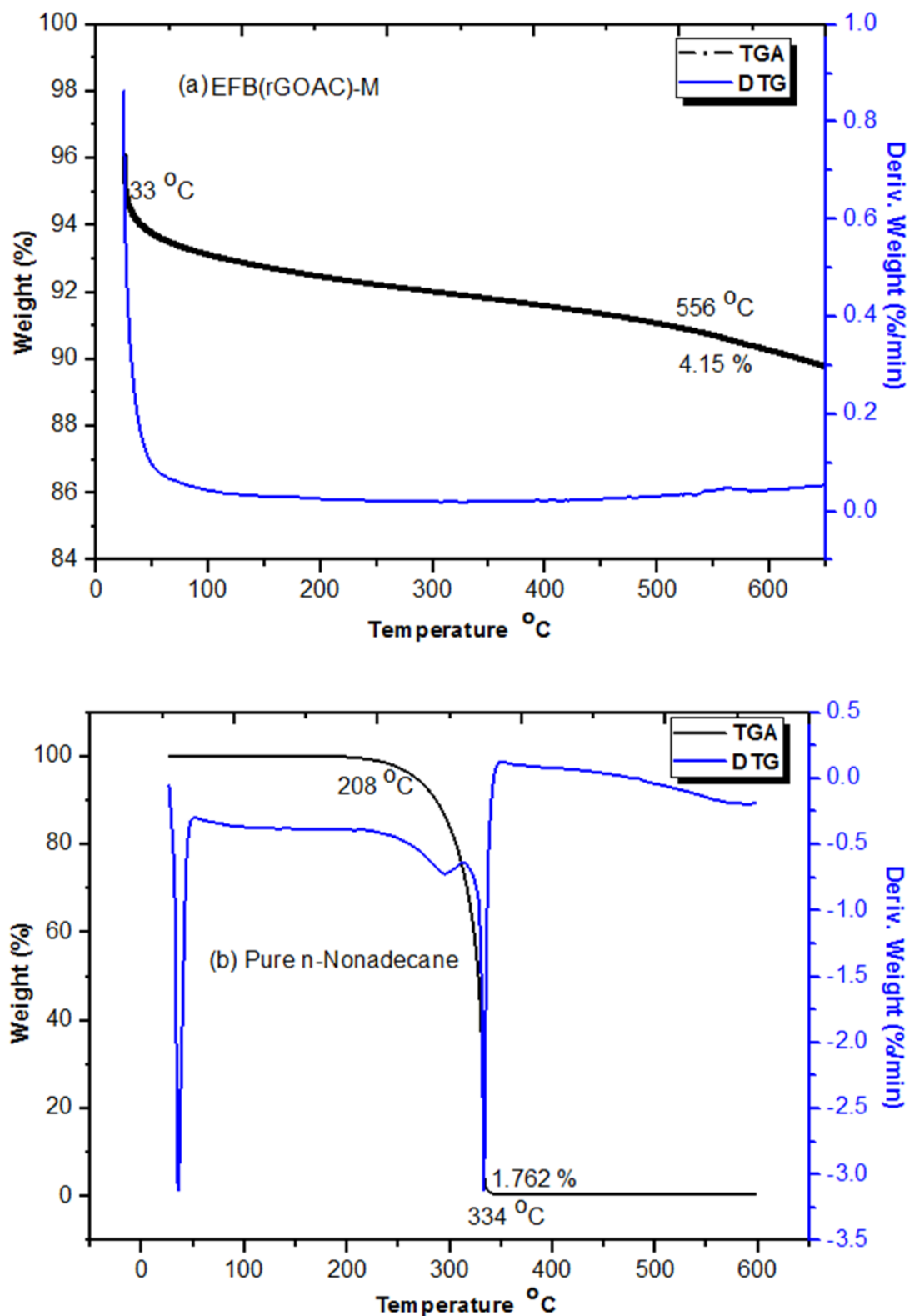


Fig. 10. TGA/DTG thermograms of (a) EFB(rGOAC)-M and (b) pure n-nonadecane

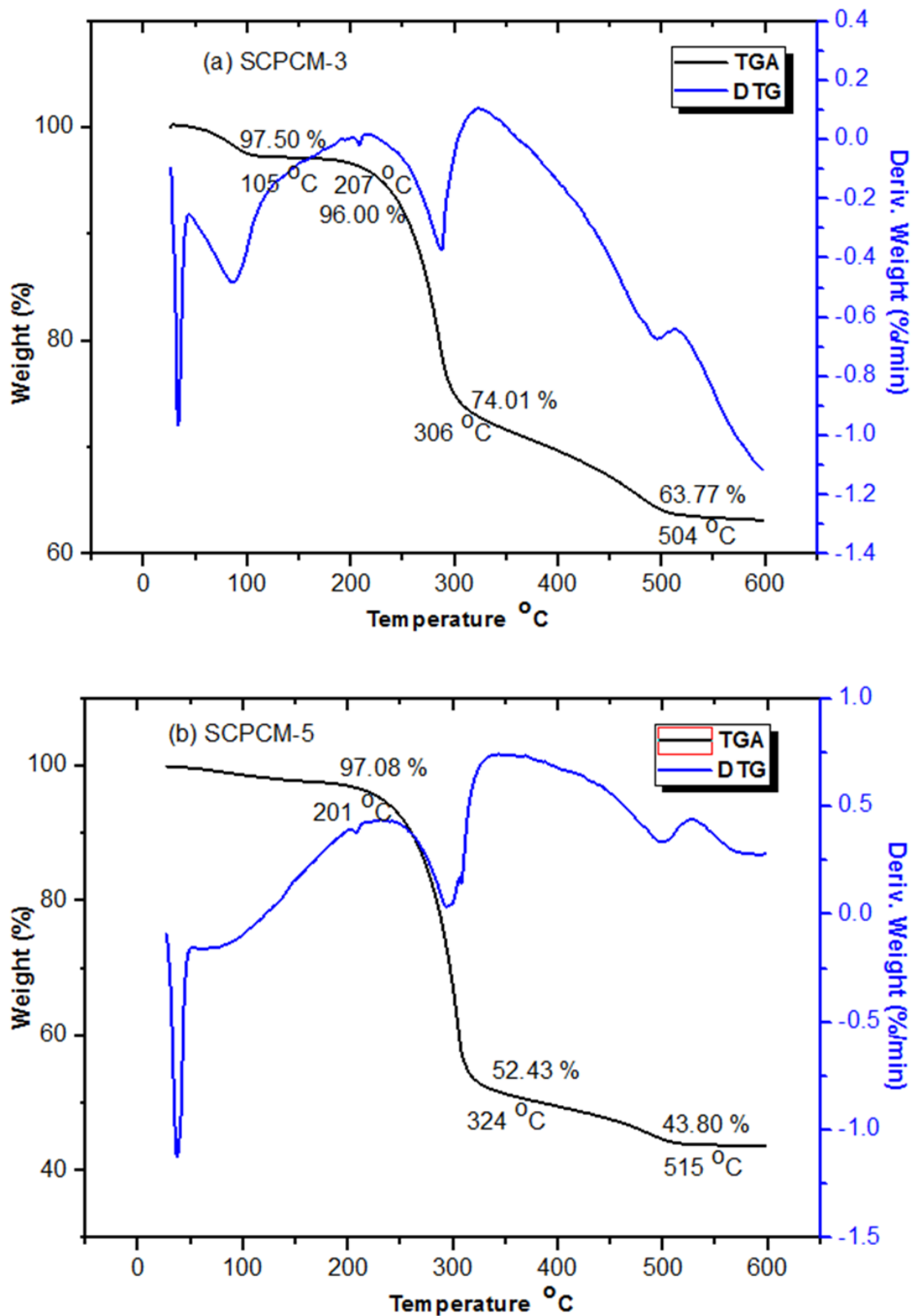


Fig. 11. TGA/DTG thermograms of (a) SCPCM-3 and (b) SCPCM-5

The carbon matrix (EFB(rGOAC)-M) forms a protective shield on the surface of the occluded or encapsulated composite PCMs; it retards the breakdown of the n-nonadecane by preventing the passage of the heat from the flame to the gas phase and the transmission of heat from the flame to the solid phase. Therefore, the reduced graphene oxide-activated carbon matrix (EFBrGOAC-M) used in this study is an excellent material that enhances the thermal stability of the composite PCM. This finding is consistent with a previous report (Mehrali *et al.* 2013).

Unlike the EFB(rGOAC)-M, the TGA/DTG curve of the pure n-nonadecane PCM (Fig. 10b) showed two-step weight losses. The first peak transpired at 208 °C, which represented the thermal decomposition of the n-nonadecane molecular chains, while the second peak surfaced at 334 °C and become depleted almost completely at this point. An overall weight loss of 98.24% (*i.e.* 100 - 1.762) between 208 °C to 334 °C (Fig. 10b) was exhibited by the n-nonadecane due to the evaporation of its contents.

The overall disintegration of the SCPCM-3 and SCPCM-5 occurred at a higher temperature than pure n-nonadecane (Fig. 11a, b).

The SCPCM-3 (Fig. 11a) started to degrade properly at 208 °C, and the maximum mass loss was seen at 504 °C, with an equivalent residual mass of 63.8%. Similarly, the degradation of SCPCM-5 (Fig. 11b) commenced at 201 °C. The maximum mass loss was recorded at 515 °C, and the resultant residual mass was 43.8%. The thermal stability of the SCPCM-5 increased in a similar pattern with EFB(rGOAC)-M (Fig. 10a). The thermal energy was initially absorbed by EFB(rGOAC)-M, and as a result, the adequate energy needed to fuel the n-nonadecane disintegration only becomes viable at a slightly higher temperature. During the decomposition of composite PCM, the surface of the carbon matrix adsorbs volatile substances, which impedes its discharge out of the sample (M.J. Mochane, 2015; Yang *et al.* 2017). For this reason, the mass loss could only be seen at a slightly higher temperature. In summary, the EFB(rGOAC)-based carbon matrix used in this investigation could be described an excellent shape-stabilized phase change material that protected the n-nonadecane during the thermal decomposition process which led to its stability.

CONCLUSIONS

1. The reduced graphene oxide-activated carbon matrix exhibited a micropore size distribution based on the IUPAC classification and showed good sorption for n-nonadecane.
2. The n-nonadecane/EFB(rGOAC) composite served as a shape-stabilized phase change material (SCPCM). It was prepared by absorbing the melted n-nonadecane into the porous structure of EFB(rGOAC)-matrix; n-nonadecane was chosen as the PCM and EFB(rGOAC)-M as the support/framework. Five different weight percentages of n-nonadecane/rGOEFBAC composite were employed in the encapsulation process (10, 30, 50, 70, and 90 wt%).
3. Lower n-nonadecane loading or concentrations led to improper encapsulation of n-nonadecane into the EFB(rGOAC)-M pores. Optimal encapsulation was achieved using 90 wt% of the composite materials in which the mixture of the reduced graphene oxide-activated carbon in the form of carbon matrix/support exhibited the maximum sorption capacity of 36% for n-nonadecane.

4. Due to the decrease in the BET surface area of the EFB(rGOAC)-M after encapsulation, and the sudden change of its isotherm profile from Type I to Type III, the n-nonadecane was shown to inhabit the pores of the material after the impregnation. The surface morphology studies corroborated these observations, indicating the perfect encapsulation.
5. The liquefied n-nonadecane PCM from the composite did not exhibit seepage while the SCPCM-5 was undergoing the phase change processes. The n-nonadecane was infiltrated into the pores of the EFB(rGOAC)-M and firmly bound by the surface tension and capillary forces of the porous carbon matrix (EFB(rGOAC)-M).
6. The phase change temperatures and latent heats of composite SCPCM-5 were 37.25 and 25.58 °C and 82.72 and -62.22 J/g, respectively.
7. The shape-stabilized composite PCM produced in this work could be utilized for energy conservation in buildings, hauling industries, temperature revitalization systems for TES and in electronic appliances, *etc.*

ACKNOWLEDGMENTS

The authors gratefully acknowledge Universiti Putra Malaysia (UPM) and the Ministry of Higher Education of Malaysia for providing the funds to conduct this research under Putra grant, GP-IPS/2018/9627200. Salisu Nasir would also like to thank the Federal University Dutse, Nigeria, for his Ph.D. study leave.

REFERENCES CITED

- Abbasi, T., and Abbasi, S. A. (2011). "Decarbonization of fossil fuels as a strategy to control global warming," *Renewable and Sustainable Energy Reviews* 15(4), 1828-1834. DOI: 10.1016/j.rser.2010.11.049
- Chen, Z., Shan, F., Cao, L., and Fang, G. (2012). "Synthesis and thermal properties of shape-stabilized lauric acid/activated carbon composites as phase change materials for thermal energy storage," *Solar Energy Materials and Solar Cells* 102, 131-136. DOI: 10.1016/j.solmat.2012.03.013
- Cui, H., Liao, W., Memon, S. A., Dong, B., and Tang, W. (2014). "Thermophysical and mechanical properties of hardened cement paste with microencapsulated phase change materials for energy storage," *Materials* 7(12), 8070-8087. DOI: 10.3390/ma7128070
- Dong, Z., Cui, H., Tang, W., Chen, D., and Wen, H. (2016). "Development of hollow steel ball macro-encapsulated PCM for thermal energy storage concrete," *Materials* 9(1). DOI: 10.3390/ma9010059
- Feng, L., Zheng, J., Yang, H., Guo, Y., Li, W., and Li, X. (2011). "Preparation and characterization of polyethylene glycol/active carbon composites as shape-stabilized phase change materials," *Solar Energy Materials and Solar Cells* 95(2), 644-650. DOI: 10.1016/j.solmat.2010.09.033
- González-García, P., Centeno, T. A., Urones-Garrote, E., Ávila-Brandé, D., and Otero-Díaz, L. C. (2013). "Microstructure and surface properties of lignocellulosic-based

- activated carbons,” *Applied Surface Science* 265, 731-737. DOI: 10.1016/j.apsusc.2012.11.092
- Hazra, S., and Basu, S. (2016). “Graphene-oxide nano composites for chemical sensor applications,” *C Journal of Carbon Research* 2(2), 1-18. DOI: 10.3390/c2020012
- Hussein, M. Z., Khadiran, T., Zainal, Z., and Rusli, R. (2015). “Properties of n-octadecane-encapsulated activated carbon nanocomposite for energy storage medium: The effect of surface area and pore structure,” *Australian Journal of Basic and Applied Sciences* 9(8), 82-88.
- Khadiran, T., Hussein, M. Z., Zainal, Z., and Rusli, R. (2015). “Activated carbon derived from peat soil as a framework for the preparation of shape-stabilized phase change material,” *Energy* 82, 468-478. DOI: 10.1016/j.energy.2015.01.057
- Khadiran, T., Hussein, M. Z., Zainal, Z., and Rusli, R. (2016). “Advanced energy storage materials for building applications and their thermal performance characterization: A review,” *Renewable and Sustainable Energy Reviews* 57, 916-928. DOI: 10.1016/j.rser.2015.12.081
- Mochane, M. J., and Luyt, A. S. (2015). “The effect of expanded graphite on the thermal stability, latent heat, and flammability properties of EVA/wax phase change blends,” *Polymer Engineering and Science*, 1-8. DOI: 10.1002/pen.24063
- Marcano, D. C., Kosynkin, D. V., Berlin, J. M., Sinitskii, A., Sun, Z., Slesarev, A., Tour, J. M. (2010). “Improved synthesis of graphene oxide,” *ACS Nano* 4(8), 4806-4814.
- Mehrali, M., Latibari, S. T., Mehrali, M., Metselaar, H. S. C., and Silakhori, M. (2013). “Shape-stabilized phase change materials with high thermal conductivity based on paraffin/graphene oxide composite,” *Energy Conversion and Management* 67, 275-282. DOI: 10.1016/j.enconman.2012.11.023
- Mehrali, M., Tahan Latibari, S., Rosen, M. A., Akhiani, A. R., Naghavi, M. S., Sadeghinezhad, E., Mehrali, M. (2016). “From rice husk to high performance shape stabilized phase change materials for thermal energy storage,” *RSC Advances* 6(51), 45595-45604. DOI: 10.1039/c6ra03721f
- Nasir, S., Hussein, M. Z., Zainal, Z., Yusof, N. A., Mohd Zobir, S. A., and Alibe, I. M. (2019). “Potential valorization of by-product materials from oil palm: A review of alternative and sustainable carbon sources for carbon-based nanomaterials synthesis,” *BioResources* 14(1), 2352-2388. DOI: 10.15376/biores.14.1.Nasir
- Nasir, S., Hussein, M. Z., Yusof, N. A., and Zainal, Z. (2017). “Oil palm waste-based precursors as a renewable and economical carbon sources for the preparation of reduced graphene oxide from graphene oxide,” *Nanomaterials* 7, 1-18. DOI: 10.3390/nano7070182
- Nasir, S., Hussein, M., Zainal, Z., Yusof, N., and Mohd Zobir, S. (2018). “Electrochemical energy storage potentials of waste biomass: Oil palm leaf- and palm kernel shell-derived activated carbons,” *Energies* 11(12), 3410. DOI: 10.3390/en11123410
- Pimenta, M. A., Dresselhaus, G., Dresselhaus, M. S., Cañado, L. G., Jorio, A., and Saito, R. (2007). “Studying disorder in graphite-based systems by Raman spectroscopy,” *Physical Chemistry Chemical Physics* 9(11), 1276-1291. DOI: 10.1039/b613962k
- Thommes, M., Kaneko, K., Neimark, A. V., Olivier, J. P., Rodriguez-Reinoso, F., Rouquerol, J., and Sing, K. S. W. (2015). “Physisorption of gases, with special reference to the evaluation of surface area and pore size distribution (IUPAC Technical Report),” *Pure and Applied Chemistry* 87(9–10), 1051-1069. DOI:

10.1515/pac-2014-1117

- U.S. Energy Information Administration (2016). *International Energy Outlook*, Washington, DC, USA.
- Waisi, B. I., Manickam, S. S., Benes, N. E., Nijmeijer, A., and Mccutcheon, J. R. (2019). “Activated carbon nanofiber nonwovens: Improving strength and surface area by tuning fabrication procedure,” *Industrial and Engineering Chemistry Research* 58(10), 4084-4089. DOI: 10.1021/acs.iecr.8b05612
- Whiffen, T. R., and Riffat, S. B. (2013). “A review of PCM technology for thermal energy storage in the built environment: Part I,” *International Journal of Low-Carbon Technologies* 8(3), 147-158. DOI: 10.1093/ijlct/cts021
- White, R. J. (ed.) (2015). *Porous Carbons from Sustainable Precursors*, The Royal Society of Chemistry, London.
- Yang, H., Memon, S. A., Bao, X., Cui, H., and Li, D. (2017). “Design and preparation of carbon based composite phase change material for energy piles,” *Materials* 10(4), 1-15. DOI: 10.3390/ma10040391
- Yu, S., Jeong, S. G., Chung, O., and Kim, S. (2014). “Bio-based PCM/carbon nanomaterials composites with enhanced thermal conductivity,” *Solar Energy Materials and Solar Cells* 120(PART B), 549-554. DOI: 10.1016/j.solmat.2013.09.037
- Zhang, L., Zhu, J., Zhou, W., Wang, J., and Wang, Y. (2012). “Thermal and electrical conductivity enhancement of graphite nanoplatelets on form-stable polyethylene glycol/polymethyl methacrylate composite phase change materials,” *Energy* 39(1), 294-302. DOI: 10.1016/j.energy.2012.01.011
- Zhang, P., Hu, Y., Song, L., Lu, H., Wang, J., and Liu, Q. (2009). “Synergistic effect of iron and intumescent flame retardant on shape-stabilized phase change material,” *Thermochimica Acta* 487(1-2), 74-79. DOI: 10.1016/j.tca.2009.01.006
- Zhao, X., Chen, H., Kong, F., Zhang, Y., Wang, S., Liu, S., Lucia, L. A., Fatehi, P., and Pang, H. (2019). “Fabrication, characteristics and applications of carbon materials with different morphologies and porous structures produced from wood liquefaction: A review,” *Chemical Engineering Journal*. DOI: 10.1016/j.cej.2019.01.159

Article submitted: April 21, 2019; Peer review completed: July 13, 2019; Revisions accepted: October 29, 2020; Published: November 9, 2020.

DOI: 10.15376/biores.16.1.96-117